A Mean Flow Model for Polymer and Fiber Turbulent Drag Reduction

Anshuman Roy and Ronald G. Larson*

Department of Chemical Engineering, University of Michigan, Ann Arbor, MI 48109, USA

*Email: rlarson@umich.edu
Fax: x1.734.763.0459

Abstract:

We present a one-parameter model that fits quantitatively the mean velocity profiles from experiments and numerical simulations of drag-reduced wall-bounded flows of dilute solutions of polymers and non-Brownian fibers in the low and modest drag reduction regime. The model is based on a viscous mechanism of drag reduction, in which either extended polymers or non-Brownian fibers increase the extensional viscosity of the fluid and thereby suppress both small and large turbulent eddies and reduce momentum transfer to the wall, resulting in drag reduction. Our model provides a rheological interpretation of the upward parallel shift S^+ in the mean velocity profile upon addition of polymer, observed by Virk. We show that Virk's correlations for the dependence on polymer molecular weight and concentration of the onset wall shear stress and slope increment on the Prandtl-Karman plot can be translated to two dimensionless numbers, namely an onset Weissenberg number and an asymptotic Trouton ratio of maximum extensional viscosity to zero-shear viscosity. We believe that our model, while simple, captures the essential features of drag reduction that are universal to flexible polymers and fibers, and, unlike the Virk phenomenology, can easily be extended to flows with inhomogeneous polymer or fiber concentration fields.

Zusammenfassung:

Wir präsentieren ein 1-Parameter-Modell, das quantitativ die mittleren Geschwindigkeitsprofile aus Experimenten und numerischen Simulationen von strömungswiderstandsreduzierenden, durch Wände begrenzte Strömungen von verdünnten Lösungen aus Polymeren und nicht-Brownschen Fasern für niedrige und mittlere Strömungswiderstände wiedergibt. Das Modell basiert auf einem viskosen Mechanismus der Widerstandsreduktion, in dem entweder ausgedehnte Polymere oder nicht-Brownsche Fasern die Dehnviskosität des Fluids erhöhen und dadurch kleine und große turbulente Wirbel unterdrücken und den Impulstransfer zur Wand reduzieren, was in eine Verminderung des Strömungswiderstandes resultiert. Unser Modell beinhaltet eine rheologische Interpretation der parallelen Aufwärtsverschiebung S+ im mittleren Geschwindigkeitsprofil bei Zugabe des Polymers, die von Virk beobachtet wurde. Wir zeigen, dass die Korrelationen von Virk für die Abhängigkeit vom Molekulargewicht des Polymers und der Konzentration der anfänglichen Wandscherspannung und der Steigung in der Prandtl-Karman-Auftragung in zwei dimensionslose Größen übertragen werden können, nämlich in eine Weissenbergzahl für den Beginn und in ein asymptotisches Trouton-Verhältnis der maximalen Dehnviskosität zur Schernullviskosität. Wir glauben, dass unser Modell, obgleich es einfach ist, die wesentlichen Merkmale der Strömungswiderstandsreduktion beinhaltet, die allgemein für flexible Polymere und Fasern gelten, und, im Gegensatz zur Phänomenologie von Virk, in einfacher Weise auf Strömungen mit inhomogenen Konzentrationsfeldern von Polymeren und Fasern erweitert werden kann.

Résumé:

Nous présentons un modèle à un paramètre qui s'ajuste quantitativement aux profils de vélocité moyenne provenant d'expériences et de simulations numériques d'écoulements avec réduction de résistance et sans glissement aux parois pour des solutions diluées de polymères et de fibres non Browniennes, dans le régime de faible réduction de résistance. Le modèle est basé sur un mécanisme visqueux de la réduction de résistance, dans lequel soit les polymères étirés, soit les fibres non Browniennes augmentent la viscosité extensionnelle du fluide, et ainsi suppriment les bords de grande ou petite turbulence, et réduisent le transfert de force vers les murs, ce qui a pour effet une réduction de la résistance. Notre modèle fournit une interprétation rhéologique du déplacement parallèle vers le haut S+ pour le profile de vélocité moyenne, observé par Virk lors de l'addition du polymère. Nous montrons que les corrélations de Vick établies pour la variation de l'apparition de contrainte aux parois et de l'augmentation de la pente sur le graphe de Prandtl-Karman en fonction du poids moléculaire du polymère et de la concentration en polymère, peuvent être réduites à deux nombres adimensionnels, à savoir un nombre de Weissenberg critique pour l'apparition de la contrainte, et un ratio de Trouton asymptotique de la viscosité extensionnelle maximum sur la viscosité statique. Nous pensons que notre modèle, malgré sa simplicité, capture les caractéristiques essentielles de la réduction de résistance qui sont universelles pour les polymères flexibles et les fibres, et, contrairement à la phénoménologie de Virk, peut aisément être étendue à des écoulements avec des champs non homogènes de concentration en polymère ou fibre.

1 INTRODUCTION

The phenomenon of turbulent skin friction drag reduction by additives finds applications in higher throughput in oil pipelines [1], and possible future applications in increased ship speeds [2] and fire fighting [3]. Despite such important applications and the fact that its existence has been known for over fifty years, the underlying physics remains murky, although much progress has been made through the use of fully three-dimensional time-dependent direct numerical simulations (DNS) of turbulent flow with constitutive equations that model the effect of polymer or fiber additives. The additives that cause drag reduction are diverse and include linear flexible polymers [4 – 6], solutions of thread-like micelles [7], and rigid rod-like fibers [8 – 11] or rod-like polymers [12, 13]. In what follows, the term "polymer" can be assumed to mean "flexible polymer," unless otherwise stated.

Many experimental investigations of drag reduction have been carried out for flexible polymers, as is summarized by Lumley [14], Virk [1] and Berman [15], but relatively few for fibers, although data are available for colloidal particles [11], asbestos fibers [16] and schizophyllum polysaccharide molecules [13], with aspect ratios varying from 25 to 10^5. An advantage of using fibers over polymers is that the former are far more resistant to mechanical degradation. The few experimental and direct numerical simulation (DNS) studies of drag reduction by fiber additives that have been performed show features that are qualitatively similar to what is observed in polymer drag reduction at low or modest levels of drag reduction, including a suppression of wall-normal velocity fluctuations, an enhancement of stream-wise velocity fluctuations, an upward parallel shift in the Newtonian "law of the wall" velocity profile and the fact that concentrations of fibers too low to significantly affect the shear viscosity of the fluid nevertheless significantly reduce drag [17]. Furthermore, fibers have been used in conjunction with polymers resulting in a synergistic drag reduction effect, larger than that obtained by polymers alone [10].

While there are no doubt differences in the detailed changes in turbulent structures produced by different types of polymers, by Brownian and non-Brownian fibers, and by thread-like micelles, the similarity in drag reduction produced by all these additives seems to call for a simplified generic explanation that encompasses them all. These additives are all long, slender objects, at least when they are extended in flow, and consequently they show high extensional viscosities, even at concentrations too low for them to significantly affect the fluid shear viscosity. Their effect on extensional viscosity is a significant clue to the general mechanism underlying their drag-reducing potency, since the extensional viscosity appears to be the only continuum rheological property that is changed enough by these additives to account for the drastic changes in flow structure that are observed. The other significant clue comes from the experimental observation that spherical particles do not produce any drag reduction [9]. And indeed, the high extensional stress in dilute polymer solutions figures prominently in the earliest phenomenological explanations of drag reduction including a "viscous" mechanism proposed by Lumley [14] and an "elastic" mechanism proposed by de Gennes [18].

In the "viscous" mechanism, which was proposed in the context of drag reduction with polymers in channel and pipe flows, turbulent flow unravels the polymer molecules, once the local strain rate exceeds the inverse of the polymer relaxation time [14]. This is the "time-scale criterion" for the onset of drag reduction. The unraveled polymer molecules increase the extensional viscosity, causing drag reduction. In channel flow, the region closest to the wall is referred to as the viscous sublayer. Beyond the viscous sublayer lies a thin buffer region of intense turbulent activity, including large scale coherent structures and bursts that result in a fluctuating extensional flow field [19, 20], superposed onto the mean shear flow. Above the buffer region is the log region in which the extensional component of the flow becomes less intense. Thus, maximum extension of polymer molecules is expected in the buffer region, which will consequently be the region with the largest extensional viscosity. Indeed, DNS studies of turbulent flow using a finitely extensible non-linear elastic (FENE-P) model [21, 22] show that the polymer can stretch to more than 80 % its fully stretched length and dramatically increase the extensional viscosity in that region. Polymers that are nearly fully stretched dissipate energy quickly, giving credence to the "viscous" mechanism.

The other phenomenological explanation for drag reduction by polymers is the "elastic" mechanism, which was originally proposed for polymer drag reduction in homogeneous, isotropic turbulence [18]. According to this view, the elasticity conferred on the fluid by the polymers interferes with the non-linear mechanism that generates the instabilities that lead to smaller length scale flows or eddies. The onset of drag reduction occurs when the polymer relaxation time exceeds the time scale associated with the smallest eddies in the flow. This is again the "time scale criterion" alluded to earlier. When the elastic energy stored in the polymer becomes comparable to the turbulent kinetic energy contained in an eddy of a certain size, all the eddies smaller than it are suppressed, leading to drag reduction. Since the elastic energy is proportional to the concentration of polymer molecules, the onset of drag reduction requires a critical polymer concentration to be present. The elastic energy corresponding to this critical concentration of polymer molecules must equal or exceed the kinetic energy associated with the smallest length scale eddies in the flow. Consequently, a "length-scale criterion" must necessarily be met by the polymer concentration in addition to the above-mentioned time-scale criterion [18]. Several comments are in order. First, a strong assumption in the elastic theory is that because the strain rates of turbulence fluctuate, the flow is unable to sustain polymer stretching long enough for the chains to approach full extension. Second, the theory demands that a critical concentration is required for the onset of drag reduction, a hypothesis not well-supported by experimental data, which instead seem to indicate that the onset of drag reduction is set by polymer molecular weight and wall shear stress. Concentration serves mainly to influence how rapidly drag reduction increases with wall shear stress once the critical wall shear stress is attained [1].

The elastic theory has also been adapted for channel flow [23]. Some verification of this adaptation may be found in direct numerical simulation (DNS) of channel flow of an Oldroyd-B fluid (which models a polymer molecule as a dumbbell with a linear Hookean spring), wherein substantial drag reduction was observed [24]. In a subsequent DNS with the same model [25], maximum drag reduction was also observed for large enough concentration of polymer and at a suffi-

ciently high Reynolds number. A budget of the space- and time-averaged turbulent kinetic energy revealed that the polymer molecules were stretched in the buffer layer, producing high levels of stored elastic energy within them. However, upon being advected away from the buffer layer into regions where the flow is not strong enough to keep them stretched, the polymer chains relax, and release the stored elastic energy back to the turbulence, thereby re-energizing it and creating an upper bound on drag reduction, or a "maximum drag reduction asymptote." But, this explanation cannot be the entire story of polymer drag reduction since these DNS results seem antithetical to Virk's phenomenological relationships [1] for polymer drag reduction, which are derived out of several data sets from a large number of experimental sources. These relationships reveal that the slope increment on the Prandtl-Karman plot (described later) is linearly dependent on the molecular weight of the polymer at fixed dimensionless shear rate or "Weissenberg number". Since the Oldroyd-B constitutive equation models an infinitely extensible chain, at fixed dimensional flow rate, or Weissenberg number, there can, for this model, be no dependence of the ensuing drag reduction on the molecular weight. Besides, the large extent of stretching observed in DNS studies of turbulent flow using a finitely extensible non-linear elastic (FENE-P) model [21, 22], suggests that the linear elastic Oldroyd-B model for the polymer molecule is unrealistic. Several other numerical investigations using the FENE-P model have reported large extension of polymer molecules in the near-wall region [21, 22, 26, 27, 28], lending support for the "viscous" mechanism.

To distinguish between the elastic and viscous mechanisms of drag reduction, it is helpful to consider DNS simulations using purely viscous constitutive equations and drag reduction by fiber additives, since these additives can greatly increase the extensional viscosity of the fluid without contributing much to the fluid's elasticity, especially if the fibers are non-Brownian. The first attempt at computationally investigating the "viscous" mechanism modeled the polymeric fluid as a generalized Newtonian fluid [29] and concluded that high biaxial extensional stress is crucial for drag reduction. In a linear stability analysis of plane Poiseuille flow, a large increase in the critical Reynolds number was observed

from the canonical value of close to 5772 for a Newtonian fluid [30] to a much higher value when a thin layer of more viscous fluid was made to coincide with the "critical" layer, which is the layer in which the phase velocity of the most unstable mode and the mean velocity are "comparable" [31]. This result suggests that a strategically placed enhancement of local viscosity suppresses secondary flow structures, and hence anticipates that local viscosification by stretched polymers might suppress turbulence. Den Toonder et al. [26] performed simulations using a simplified purely viscous constitutive equation for rigid rods. They observed smaller drag reduction upon adding an ad-hoc elastic term to the purely viscous (approximate) constitutive model, thereby converting it into an anisotropic analogue of the linear Maxwell model for viscoelastic materials. Due to limitations in computing capability, very low drag reductions were achieved both with the purely viscous and the viscoelastic constitutive models. Recently, the Stanford group has published channel flow DNS results for rigid rods [17], in which fairly large drag reduction (up to 26 %) was observed for the case of non-Brownian fibers that correspond to the limit of high Peclet number, $Pe \gg 1$. Weakly elastic Brownian fibers that correspond to smaller Pe resulted in smaller drag reduction relative to non-Brownian fibers.

From DNS simulations of both turbulent flows and simpler "model" flows, some mechanistic understanding of polymer and fiber drag reduction seems to be emerging. Substantial modification in the dynamics of a model theoretical three-dimensional steady flow in the plane Couette geometry, due to large extension of polymer molecules, has been reported by Graham and co-workers [19], resulting in drag reduction [32]. These flows consist of counter-rotating streamwise coherent structures that are believed to contain all the skeletal features of the streamwise coherent structures observed in the buffer layer of fully turbulent flows [33]. It has been demonstrated that in wall-bounded flows, these coherent structures are the dominant cause of skin friction [34]. In these coherent structures, fibers get oriented while polymers get both stretched and oriented. This interferes with the self-sustaining process that maintains the coherent structures, and thereby leads to drag reduction [17, 19, 20].

If the flow local to a polymer molecule contains a dominant and persistent extensional component, polymer molecules can reach significant fraction (50-80%) of complete extension. In this limit, they may be approximated as rods, since at nearly full extension, energy from drag forces cannot further stretch the molecules and is dissipated rather than stored in further polymer stretch. But unlike rigid fibers, polymers are elastic and can relax from the extended state if the extensional strain rate of the fluid element carrying the polymer molecule decreases or the flow becomes dominantly rotational - a frequent scenario in turbulent flow as the polymer molecules are advected in an inhomogeneous flow field. Recoil of polymer molecules can transfer elastic energy from the polymer back into the turbulent flow and consequently, partly counteract the drag reducing effects of the polymer [20, 24]. The details of this transfer back of energy are different for the Oldroyd-B and the FENE-P models. In the Oldroyd-B model, there is no limit on polymer stretch, and so energy storage can dominate over dissipation no matter how much the polymers are stretched. In fact, it is observed that the polymer dissipation term, a space-time average of the fluctuating polymer stress and fluctuating velocity gradient, in the turbulent kinetic energy balance becomes positive beyond the buffer layer, thereby indicating a transfer of stored energy from the polymer back to the turbulence. In the FENE-P model, this polymer dissipation term does not become positive [28]. The Stanford group has claimed that in the case of the FENE-P model, transfer back of energy to the flow is a rare event that cannot be captured in an averaged turbulent kinetic energy budget. Still, in essence, elasticity of the polymer can be implicated for transfer of energy back to turbulence and consequently, drag enhancement, or rather, a limitation on drag reduction. Similarly, Brownian fibers are weakly elastic owing to their rotational degrees of freedom, and this elasticity results in a slightly smaller amount of drag reduction than would be obtained by non-Brownian fibers alone. Thus, direct numerical simulations suggest that drag reduction can occur in the absence of elasticity and is due to purely orientational effects of stretched out polymer molecules and fibers, that produces high extensional viscosities in regions of the flow that contain extensional kinematics, i.e., in the buffer layer
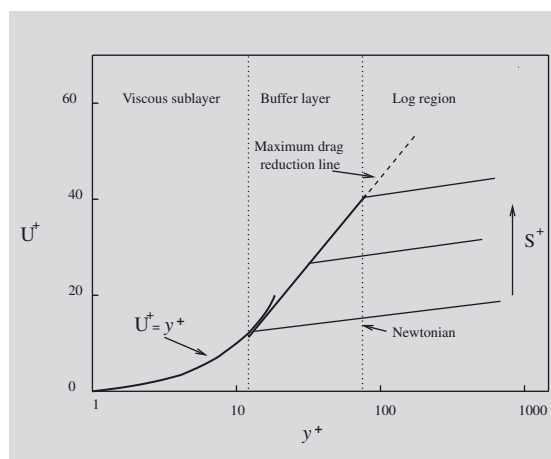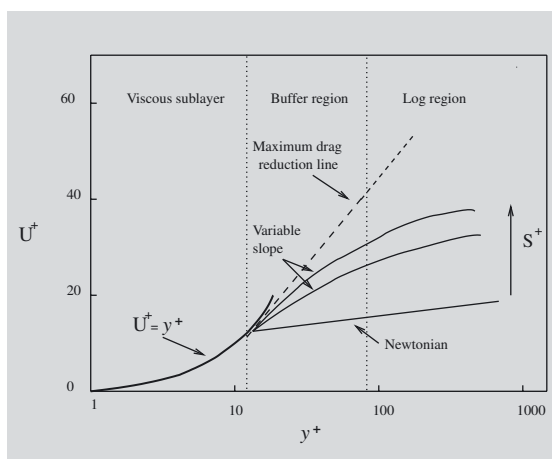
and above. The presence of elasticity actually decreases the extent of drag reduction by providing a means of storing mechanical energy that can then re-energize turbulent structures.

Hence the weight of evidence from numerical simulations of fibers and polymers more strongly supports the "viscous" mechanism than the "elastic" mechanism for drag reduction, while consigning elasticity to a spoiler's role of actually reducing the level of drag reduction that would be obtained for a fluid with the same extensional viscosity, but no elasticity. Any phenomenological model for fiber and turbulent drag reduction should therefore be based on the viscous mechanism and be able to explain, or at least rationalize, the form of the mean velocity profile that results from drag reduction. Based on the percentage of drag reduction, there are two regimes of drag reduction called low/modest (< 35 %) and high drag reduction (> 35 %) [35]. Both in experiments and direct numerical simulations of channel or pipe flows of both polymers and fibers, similar mean velocity profiles are observed in each of these regimes for all drag reducing additives; figure 1 shows a schematic mean velocity profile in the low/modest drag reduction regime. In figure 1, the viscous sublayer is the region between the wall and y^+ = 11.6. Here we reduce variables to dimensionless "+" (or "turbulent wall") units, which are defined shortly. For low and high polymer drag reduction, and fiber drag reduction, the viscous sublayer remains unchanged from Newtonian flow. Beyond the viscous sublayer lies the buffer layer, which is a relatively thin region, relative to the dimension of the channel/pipe, of about 25 wall units in Newtonian flows. In low and high polymer drag reduction regimes, and fiber drag reduction, the presence of polymer/fiber makes the buffer layer grow in spatial extent, with the slope of the mean velocity profile being dependent on the polymer molecular weight/fiber size, polymer/fiber concentration and, specifically for the case of fibers, their aspect ratio. As we mentioned earlier, the buffer layer is also the region that contains large scale coherent structures and streaks, chiefly responsible for skin friction in wall-bounded flows,

and containing patches of strongly extensional flow. Polymers have been known to modify these coherent structures and to increase the streak spacing [19, 36]. In the log region, which is the region beyond the buffer layer, the slope of the mean velocity profile in low polymer drag reduction and fiber drag reduction peters out to the Newtonian value, only shifted upwards. However in the case of high polymer drag reduction, the mean velocity profile does not peter out to the Newtonian value as in the case of low polymer drag reduction. Instead, it remains the same as in the buffer layer or only slightly altered, resulting in a "fan-type" mean velocity profile. The turbulence statistics in low and high polymer drag reduction regimes are also different. In the low drag reduction regime, the streamwise fluctuating velocity (u'^+) increases from the Newtonian value, particularly in the buffer layer, while the wall-normal fluctuating velocity (v'^+) decreases over the entire cross section of the channel. For the case of high drag reduction, both the streamwise and wall-normal fluctuating velocities decrease over the entire channel [35].

Several expressions have been developed to predict the mean velocity profile in polymer drag reduced flow, probably the most popular one being Virk's mean flow model based on his phenomenological relationships [1]. However, Virk's model is highly approximate and assumes the same slope in the buffer layer regardless of polymer concentration and molecular weight, as shown in Fig. 2. Recently, an empirical model for surfactant drag reduction has been proposed, in which the three model parameters can be adjusted to fit the data on mean velocity from experiments [37]. However, the numerical values of these parameters depends on the rheology of the fluid in an unknown way. There are no models that predict the mean velocity profile for non-Brownian fiber drag reduction. Given the similarities in the shapes of the mean velocity profiles obtained both with polymers in the low drag reduction regime and fibers, and the fact that both these additives perhaps have similar physics of drag reduction, it seems reasonable to expect that the same phenomenological model

should be able predict the mean velocity profile after drag reduction by polymers of known molecular weight or fibers of a given length and aspect ratio and concentration. Such a model would be extremely useful in developing closure models for polymer turbulent drag reduction, and consequently, solving mass and heat transfer problems in such turbulent flows. It is even more desirable to construct a mean flow model that is consistent with Virk's phenomenology and is founded on the physics of the viscous mechanism of drag reduction. Here, we present a simplified mean flow model that is based on the following key ideas:

1. Drag reduction is produced by a viscous mechanism: turbulent structures acting on polymers or fibers viscosify the fluid so as to suppress those structures.
2. The largest eddies must be suppressed to reduce turbulent momentum transport.
3. The two key rheological parameters are a Weissenberg number and a viscosity parameter, with our model focusing on the Weissenberg number defined using the local large eddy turn-over time and the viscosity parameter defined as nL^3, motivated by the Batchelor formula for extensional viscosity.

In the following sections, we first re-interpret the Virk phenomenology (mean flow model and experimental correlations) in rheological terms and show how it suggests the viscous mechanism. We then construct a mean flow model on the basis of the viscous mechanism, valid for both polymer and non-Brownian fiber drag reduction.

2 RE-INTERPRETATION OF THE VIRK PHENOMENOLOGY FOR POLYMER DRAG REDUCTION

Virk's comprehensive analysis of many sets of experimental data on polymer drag reduction for pipe and channel flows can be summed up as follows. Below a critical wall shear stress, there is no observed drag reduction; a Prandtl-Karman (PK) plot of $1/\sqrt{f}$ vs. $Re\sqrt{f}$ shows no change from ordinary turbulent flow (see Fig. 3). Here f is called Fanning's friction factor, and by definition $f \equiv 2\tau_w/\rho U^2_{av}$, where τ_w is the wall shear stress, U_{av} is the mean fluid velocity in the flow direction averaged across the cross-section of the pipe and ρ is the fluid density. Re is the Reynolds number and in this case is defined as, $Re = dU_{av}/\nu_s$, where d is the pipe diameter and ν_s is the kine-
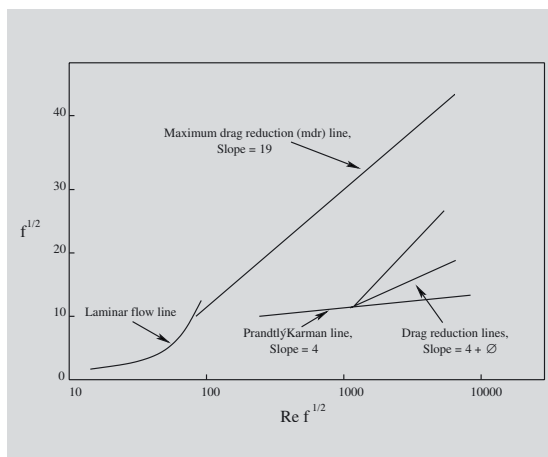
matic viscosity of the fluid. For well-developed turbulence ($Re \geq 3000$), the PK plot is given by

$$\frac{1}{\sqrt{f}} = 4.0 \log_{10}\left(Re\sqrt{f}\right) - 0.4$$

(1)

which is the straight line labeled "Prandtl-Karman line" shown in Fig. 3. With polymer, drag reduction occurs once a critical wall shear stress τ^*_w is exceeded, which depends on the radius of gyration R_G of the polymer as

$$\tau^*_w = \Omega_T R_G^{-3}$$

(2)

with τ^*_w in units of Pa and R_G in units of nm, the coefficient Ω_T has the value $4.4 \cdot 10^6$ Pa·nm³. Once this critical wall shear stress is exceeded, the slope of the PK plot in the region of well-developed turbulence changes by Δ, the slope increment, so that

$$\frac{1}{\sqrt{f}} = \left(4.0 + \Delta\right) \log_{10}\left(Re\sqrt{f}\right) - 0.4 - \Delta \log_{10}\left(Re\sqrt{f^*}\right)$$

(3)

where $(Re\sqrt{f})^*$ is the value of $Re\sqrt{f}$ at the critical stress τ^*_w at which the onset of drag reduction occurs, shown in Fig. 3. The magnitude of the slope increment Δ increases with polymer concentration and molecular weight according to

$$\Delta = \varpi N^{3/2}\left(\frac{c}{M_w}\right)^{1/2}$$

(4)

where N is the number of backbone bonds in the polymer, M_w is its weight-averaged molecular weight (in g/mole) and c is the concentration in units of ppm. Hence, the phenomenological coefficient ϖ is dimensional, and has a value of around $70 \cdot 10^{-6}$ in the appropriate units. At high Reynolds number, there is a maximum drag reduction (mdr) asymptote, given by,

$$\frac{1}{\sqrt{f}} = 19.0 \log_{10}\left(\text{Re}\sqrt{f}\right) - 32.4 \tag{5}$$

With drag reduction, changes in the mean velocity profile accompany changes in the PK plot. Virk assumes a two-layer mean flow model for the mean velocity profile and ignores the buffer layer in the absence of drag reduction [38]. Thus, for $y^+ < 11.6$,

$$U^+ = y^+ \tag{6}$$

and for $y^+ > 11.6$

$$U^+ = 2.5\ln y^+ + 5.5 \tag{7}$$

where the mean streamwise velocity U^+ is measured in units of the turbulent velocity scale, $u_T = (\tau_w/\rho)^{1/2}$ and the distance normal to the wall y^+ is measured in units of the turbulent length scale, ν_s/u_T. Equation 6 corresponds to the viscous sublayer and Eq. 7, to the log region. According to Virk's mean flow model for polymer drag reduction, in the presence of polymer the velocity profile in the log region is shifted upwards by an amount S^+ with no change of slope, so that Eq. 7 becomes:

$$U^+ = 2.5\ln y^+ + 5.5 + S^+ \tag{8}$$

and a polymer-modified buffer layer significantly thicker than the Newtonian buffer layer (which is ignored in the two-layer formulation) is introduced, obeying

$$U^+ = 11.7\ln y^+ + 17.0 \tag{9}$$

As shown in Fig. 2, the straight line given by Eq. 9 for the buffer layer connects the curve for the viscous sublayer, Eq. 6, to the straight line for the shifted log region, Eq. 7. The upward shift in the equation for the mean velocity profile in the log region, Eq. 8, is related to the change in slope Δ of the turbulent region of the PK plot by

$$S^+ = \sqrt{2}\Delta\log_{10}\left(\frac{u_T}{u^*_T}\right) \tag{10}$$

where u^*_T is the turbulent velocity scale at the critical wall shear stress, τ^*_w, for drag reduction, $u^*_T \equiv \sqrt{(\tau^*_w/\rho)}$. In the limit of maximum drag reduction, Eq. 9 apparently applies throughout the region $y^+ > 11.6$ up to the center of the channel/pipe; i.e. there is no reversion back to Eq. 8 for the turbulent core.

Since polymer molecules are typically no longer than the smallest turbulent structures, the action of the polymer is affected through the changes it exerts on the continuum rheological properties of the fluid. Hence, Virk's phenomenology, expressed in terms of polymer molecular properties in Eqs. 2 and 4, should be expressible in terms of the rheological properties of the polymer solution. To provide a rheological interpretation of the above phenomenological description, we convert Eqs. 2 and 4 above into equations involving constitutive-level quantities, namely relaxation times and viscosities. We start by defining the turbulence-based Weissenberg number,

$$Wi_{\tau o} = \frac{\lambda u_T^2}{\nu_o} \tag{11}$$

where ν_o is the zero-shear viscosity of the fluid and λ is an effective fluid relaxation time, which for dilute solutions is related to the intrinsic viscosity $[\mu]_o$ of the polymer by

$$\lambda = K_\lambda \frac{M_w[\mu]_o \mu_s}{N_A k_B T} \tag{12}$$

where μ_s is the solvent viscosity, M_w is the weight-averaged polymer molecular weight, N_A is Avogadro's number, k_B is Boltzmann's constant, T is the absolute temperature, and K_λ is a constant of order unity that expresses the width of the relaxation spectrum. Note that here we depart from the usual notation for the intrinsic viscosity of polymer solution which is $[\eta]_o$ so as to be able to use the symbol η to represent the Kolmogorov length scale later on. For a single-relaxation-time model such as the so-called FENE-P model [39], K_λ is unity. Next, we note that the intrinsic viscosity is related to the polymer radius of gyration by [1]

$$R_G^3 = \frac{HM_w[\mu]_o}{31\cdot10^{23}} \tag{13}$$

where H, the "heterogeneity index", is the ratio of third to second moments of the molecular weight distribution. Combining Eqs. 11, 12, and 13:

$$Wi^*_{\tau O} = K_\lambda \frac{31\cdot10^{23}}{HN_A k_B T} R_G^3 \tau^*_w \tag{14}$$

For temperatures in the vicinity of room temperature, $k_B T = 4.11\cdot10^{-21}$J. Expressing R_G in nm and τ_w in Pa, and using Eq. 2, we obtain

$$Wi^*_{\tau O} = \frac{5.5K_\lambda}{H} \tag{15}$$

where $Wi^*_{\tau O}$ is the critical Weissenberg number for drag reduction. Thus, for a monodisperse polymer (H = 1) described by a single relaxation time (K_λ = 1), the critical Weissenberg number for the onset of drag reduction should be around 5, or so, in rough agreement with recent direct numerical simulations [21]. The arguments above closely follow Lumley's [14] onset condition as well. He suggested that the onset of drag reduction occurs only after $Wi^*_{\tau O} \sim O(1)$.

Once this critical Weissenberg number is exceeded, the magnitude of drag reduction depends on the slope increment Δ, given by Eq. 4. We first convert the concentration c in this formula into the number of polymer molecules per unit volume n

$$c(ppm) = \frac{nM_w}{\rho N_A}\cdot10^6 \tag{16}$$

where the factor of 10^6 converts mass fraction into ppm. The length of a fully extended polymer molecule L is related to the number of backbone bonds N by

$$L = 0.82Nl \tag{17}$$

where l is the length of a backbone bond, 1.54 Å for a carbon-carbon bond, and the factor of 0.82 accounts for the typical zigzag conformation of a fully extended polymer chain with tetrahedral

bonding of the backbone atoms. With this information, Eq. 4 becomes:

$$\Delta = 0.064\left(nL^3\right)^{1/2} \tag{18}$$

The asymptotic extensional viscosity of fluid, when polymer chains are fully extended, can be estimated by a formula for rigid rods due to Batchelor [40]:

$$\bar{\mu}_\infty = \frac{\pi}{6\ln(2L/a)}\mu_s nL^3 \approx \frac{1}{20}\mu_s nL^3 \tag{19}$$

where a is the diameter of the extended polymer filament. In Eq. 19, we neglect the contribution of the solvent to the extensional viscosity of the solution, since it is typically negligible compared to the polymer contribution when the polymer is fully extended in an extensional flow. Since the logarithm in Eq. 19 is very weakly dependent on chain length, we have substituted a typical value, 10, into Eq. 19. Combining this with Eq. 18 gives a relationship between Δ and $\bar{\mu}_\infty$:

$$\Delta = 0.286\left(\frac{\bar{\mu}_\infty}{\mu_s}\right)^{1/2} \tag{20}$$

Equation 20 implies that higher extensional viscosities, obtained by either higher molecular weights, or higher concentrations of polymer, lead to greater drag reduction once the critical Weissenberg number (or critical stress) is exceeded. Since the ratio $\bar{\mu}_\infty/\mu_s$ is related to the aymptotic Trouton ratio,

$$Tr \equiv \frac{\bar{\mu}_\infty}{\mu_o} \tag{21}$$

by $Tr/\beta = \bar{\mu}_\infty/\mu_s$, where $\beta = \mu_s/\mu_O$ is the ratio of the solvent to the zero-shear viscosity of the solution, we re-cast the relationship for the parallel upward shift, Eq. 10 in terms of Tr, $Wi_{\tau O}$ and $Wi^*_{\tau O}$ as

$$S^+ = 0.2\left(\frac{Tr}{\beta}\right)^{1/2}\log_{10}\left(\frac{Wi_{\tau O}}{Wi^*_{\tau O}}\right) \tag{22}$$

Equations 15 and 22 provide us with the sought-after relationships between drag-reduction phenomenology and constitutive properties of the fluid, since we have now expressed the critical wall shear stress as a critical Weissenberg number ($Wi^*_{\tau O}$), and the slope enhancement Δ as a function of the asymptotic Trouton ratio (Tr) of the fluid. The appearance of $Wi^*_{\tau O}$ and Tr in our interpretation and no term corresponding to stored elastic energy, shows that the Virk phenomenology is consistent with the "viscous" mechanism, rather than the "elastic" mechanism. Onset of drag reduction occurs once $Wi_{\tau O} > Wi^*_{\tau O}$ implying that the polymer molecules unravel. Once they begin to unravel, the polymer molecules would have to stretch up to a large fraction ($> 1/3$) of complete extension in order for the fluid to feel the asymptotic extensional viscosity. Ryskin [41] came up with a similar argument for connecting the slope increment in the PK plot to polymer parameters based on his "yo-yo" model for polymer extension in fast transient flows.

Although we have shown that Virk's correlations can be translated into rheological quantities, a few words need to be said about the uncertainties regarding the data he used to arrive at his correlations. We re-iterate that his correlations are based on data from polydisperse polymer solutions, several of which might have been poorly characterized. At the time these experiments were performed, only indirect means of characterizing the polymer solutions existed and only polydisperse polymer samples were commonly available for experiments. Polydispersity of polymer samples and a lack of the knowledge of the accompanying molecular weight distribution required the use of a weight-averaged molecular weight, M_w, in all the correlations. This could skew the correlations, if, for example, only the few chains with very high molecular weight in the population of chains stretch out and are entirely responsible for drag reduction. Also, the choice of relaxation time for computing the Weissenberg number is in doubt, since some recent experiments have shown a strong dependence of fluid relaxation time on the concentration of polymer molecules in the solution, even in the so-called dilute limit [42].

Finally, in turbulent flow some mechanical degradation of polymer molecules is inevitably expected. So, one needs to check the effect degradation will have on Virk's correlations. To our knowledge, this has not yet been done. Hence, there remains a cloud of doubt regarding the accuracy of the correlations, which will only be dispersed once careful experiments are performed with directly characterized monodisperse polymer solutions for which the relaxation times are directly measured. Still, direct numerical simulations based on the FENE-P model have shown a good qualitative agreement with the Virk correlations in channel flow, including prediction of a critical $Wi^*_{\tau O}$ of around $Wi^*_{\tau O} \simeq 5$, and an upward shift in the Prandtl-Karman line with increasing polymer concentration [28, 21].

Therefore, in this work, we develop a more detailed phenomenology that is consistent with the Virk correlations that captures the "universal" features of drag reduction by extended or extensible additives (i.e., polymers and fibers), and that can be applied to more general turbulent flows, including flows over flat plates, or flows with non-uniform polymer concentration. It may be that, like Virk's correlations, our theory will work best for polydisperse polymers, but these are the ones most often used in applications. Our goal now is to construct a model for the mean velocity profile following low drag reduction due to polymers and non-Brownian fibers (shown in Fig. 1b), in which the rheological dimensionless variables, Tr and $Wi^*_{\tau O}$, appear as the key parameters.

3 MEAN VELOCITY PROFILE OF NEWTONIAN FLOW IN A CHANNEL

Before setting to the task of developing a model for the mean velocity profile in a drag-reduced channel flow, we need to develop an expression for the mean velocity profile in Newtonian channel flow that is valid both in the buffer layer as well as the log region. Since the mean velocity profile in the viscous sublayer remains unaltered following drag reduction, i.e. the same as Eq. 6, as seen both experimentally and in simulations, here we discuss the profiles in the buffer and log regions, i.e. in the region $y^+ > 11.6$.

To develop a model for the mean velocity profile beyond the viscous sublayer, consider the time and length scales of Newtonian turbulence in the log region where the "law of the wall" holds. In this region, there is thought to be a Kol-

mogorov-like cascade of eddy sizes that extends from an inertia-dominated length scale, l, to a viscosity-dominated one η. (Note that we are here using the symbol η to represent a length scale rather than a viscosity.) The former is called the integral length scale and the latter is the Kolmogorov length scale. The log region is by definition thin compared to the pipe or channel diameter; hence the integral length scale l cannot be set by the channel diameter, and since the viscous length scale cannot enter, the only remaining source of a length scale is the distance y to the wall. Thus, $l = \kappa y$, with κ a dimensionless constant. The viscous length scale is set by the kinematic viscosity, ν_s, and the mean rate of turbulent kinetic energy dissipation, $\langle \epsilon \rangle$, is given by dimensional analysis as $\eta = \nu_s^{3/4} \langle \epsilon \rangle^{-1/4}$ [43]. For wall-bounded flows, by definition [44]:

$$\langle \epsilon \rangle \equiv \frac{u_T^2}{\theta(l)} \tag{23}$$

where $\theta(l)$ is the time-scale associated with the largest eddy of size l. For the turbulent flow of a Newtonian fluid, this time-scale is set by the velocity charactersitic of the largest eddy, i.e. the turbulent velocity scale u_T, and by l itself, $\theta(l) = l/u_T$. Substituting this into Eq. 23, we obtain:

$$\langle \epsilon \rangle \equiv \frac{u_T^3}{l} \tag{24}$$

Then, putting the above formula for energy dissipation into the formula for η, we find that in the log region, there is a band of turbulent eddy sizes covering the range η to l, with

$$\eta = \nu_s^{3/4} u_T^{3/4} (\kappa y)^{1/4}; \quad l = \kappa y \tag{25}$$

The width of the band of eddy sizes therefore increases as $y^{3/4}$ with increasing distance from the wall as shown in Fig. 4. Turbulent momentum transport beyond the viscous sublayer is set by the largest eddies. This is a consequence of the development of a large gap between the largest eddy size and the smallest one, at which viscous dissipation occurs. The size of this gap can be estimated from Fig. 4, which shows that the law of the wall is only fully established at a distance of
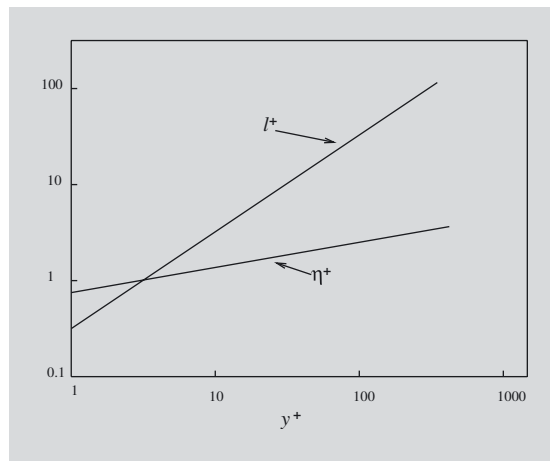
around 30 wall units. It is apparent in Fig. 4 that at this distance there is almost a decade separation between the integral scale and the Kolmogorov scale.

This large gap means that the dynamics at the small dissipation length scale can not be correlated over a long enough range to greatly influence the behavior of the large eddies, which are the ones that generate the most momentum transport. Hence, figuratively speaking, large eddies generate turbulent energy without caring how this energy is to be dissipated; they merely hand off the energy to smaller eddies and let them worry about what to do with it. However, this is not the case for regions close enough to the wall where the sizes of the largest (and most energetic) and smallest (and most dissipative) structures in the flow are separated by less than a decade [20].

Having described the general eddy picture, let us examine the streamwise mean momentum balance in channel flow, which is a balance of the Reynolds and viscous stresses:

$$-\rho \langle uv \rangle + \mu_s \frac{dU}{dy} = \tau_w \left(1 - \frac{y}{h} \right) \tag{26}$$

In the above equation, $-\rho \langle uv \rangle$ is the Reynolds stress, ρ is the fluid density, μ_s is its viscosity, $\tau_w = \mu_s (dU/dy)_{wall} = \rho u_T^2$ is the shear stress at the wall and h is the half-height of the channel. The Reynolds stress term needs to be modeled in order to solve the above equation and extract the mean velocity profile from it. Now, one of the simplest models for the turbulent transport of momentum by large eddies is that of turbulent diffusion dependent on a spatially-varying eddy viscosity defined by

$$\nu_T = \frac{l^2}{\theta(l)} \tag{27}$$

giving a simple model for the Reynolds stress:

$$-\langle uv \rangle = \nu_T \frac{dU}{dy}$$

(28)

Substituting Eq. 28 into Eq. 26 and assuming $y \ll h$ gives an expression for dU/dy:

$$\frac{dU}{dy} = \frac{u_T^2}{\nu_s + \nu_T} = \frac{u_T^2}{\nu_s + l^2 / \theta(l)}$$

(29)

To integrate this equation, we need an expression for $\theta(l)$. On dimensional grounds, it is usual to consider $\theta(l) = l/u_T$, in other words, the time scale of the largest eddies is set by its size and turn-over velocity, the latter being given by u_T. Substituting this expression into Eq. 29 and assuming $\nu_s \ll \nu_T$ results in the logarithmic expression for the mean velocity profile, Eq. 7. But here, we are interested in developing an expression that is also valid in the thin buffer layer between the viscous and log regions. We wish to incorporate the buffer layer into the expression, because of its importance in the case of drag reduction, which is addressed in the next section. In the buffer layer, which is less than 30 wall units from the wall for Newtonian turbulence, one may suppose that the large eddies are not large enough so as to remain unaffected by the dynamics of the smallest eddies. A verification of this argument comes from recent direct numerical simulations of Newtonian wall-bounded flows, in which the largest and the smallest structures in this layer were found to be separated in size by only an order of magnitude [20]. The above argument motivates the following expression:

$$\theta(l) = \frac{l}{u_T} \left(1 + \alpha \frac{\eta}{l} \right)$$

(30)

where α is a model parameter and the extra term η/l may be thought of as a higher order correction to the standard relationship for $\theta(l) = l/u_T$. We have made this correction in order to incorporate the dynamical effect of the smallest eddies on the largest eddies, near enough to the wall. Thus, in this region due to the shallowness of the turbulent cascade, the largest eddies cannot simply hand over the kinetic energy to the smaller eddies without getting affected in the process. The expression in Eq. 30 is not meant to

displace other phenomenological models for the mean flow in the buffer layer, for instance, the van Driest model. Instead, we have developed this simple expression for ease of inclusion of the effect of polymers on the turbulence cascade, and consequently drag reduction, in a transparent manner, as will be evident in the next section. The van Driest expression could be used also, but with some greater difficulty and so we leave this to future work.

Scaling the above equation in units of wall time and length scales $-u_T^2/\nu_s$ and u_T/ν_s, and using Eq. 25 we get:

$$\theta^+ = \kappa y^+ \left(1 + \frac{\alpha}{\kappa y^+} \theta^{+1/4} (3\beta)^{3/4} \right)$$

(31)

In the above equation, a factor of $(3\beta)^{3/4}$ appears, consistent with the value of the Trouton ratio of a Newtonian fluid ($\beta = 1$), in preparation of extending the model for drag reduction. Rescaling Eq. 29 we have the following relationship for the dimensionless mean velocity gradient:

$$\frac{dU^+}{dy^+} = \frac{1}{1 + (\kappa y^+)^2 / \theta^+}$$

(32)

Integrating the above equation numerically using Eq. 31 and the boundary condition that $U^+ = 11.6$ at $y^+ = 11.6$ gives us the Newtonian mean velocity profile for $y^+ > 11.6$. Since for $y^+ \gg 11.6$, the integrated form of Eq. 32 must reduce to Eq. 7, we conclude that $\alpha = 0.26$. The computed mean velocity profile is shown in Fig. 5.

4 MEAN VELOCITY PROFILE WITH DRAG REDUCTION IN A CHANNEL

Having developed a simple expression for the mean velocity profile in Newtonian flows that includes the buffer layer, we now proceed to develop a model for the mean velocity profile in channel, pipe or boundary layer flows including the effects of drag reduction. Specifically, we address the low to medium drag reduction regime for polymers and for non-Brownian fibers, where we believe that the "viscous" mechanism provides a reasonable qualitative model that can describe both fibers and polymers.

Since the largest eddies transport most of the momentum, turbulent drag cannot be

changed unless the behavior of these large eddies is somehow moderated [14]. Now, polymer molecules even when fully extended, are smaller than or about the size of the smallest eddies, depending on the Reynolds number. Although fibers larger than the Kolmogorov length scale have been used to reduce drag, here we consider drag reduction due to fibers of size smaller than the Kolmogorov length scale, which is the case considered in recent DNS studies by the Stanford group [17]. So the influence of polymer or fiber on the large eddies must be indirect. One way this influence can be exerted is through a competition of time scales, which we consider for polymers.

4.1 TIME-SCALE CRITERION IN DRAG REDUCTION WITH POLYMERS

An eddy of size r that lies between the maximum size l and the minimum size η has a characteristic time scale, or "eddy turnover time", that by dimensional analysis follows the law [45]:

$$\theta(r) \equiv \left(\frac{r^2}{\langle \epsilon \rangle} \right)^{1/3}$$

(33)

where we absorb the pre-factor into the definition of $\theta(r)$. Then the range of time constants from eddies of smallest ($r = \eta$) to largest ($r = l$) size, using Eq. 25, is

$$\theta(\eta) = \nu_s^{1/2} u_T^{-3/2} (\kappa y)^{1/2} \qquad \theta(l) = u_T^{-1} \kappa y$$

(34)

Thus, the range of eddy turnover timescales increases with distance from the wall, with the longest of these scaling linearly with distance from the wall.

How does the addition of polymer affect these time-scales? An important clue is the observation that no drag reduction is observed unless a critical value of the wall shear stress, or equivalently, a critical value of the Weissenberg number $Wi_{\tau O}$, is exceeded. The critical $Wi_{\tau O} = Wi^*_{\tau O} \approx 5$ [21] for a single-mode FENE-P model [39] and in experiments, is $Wi^*_{\tau O} \approx 1$ [1]. This is reasonable, since the contribution of the polymer to the stress in the fluid is negligible unless the polymer is stretched, which will only be the case when the velocity gradient exceeds
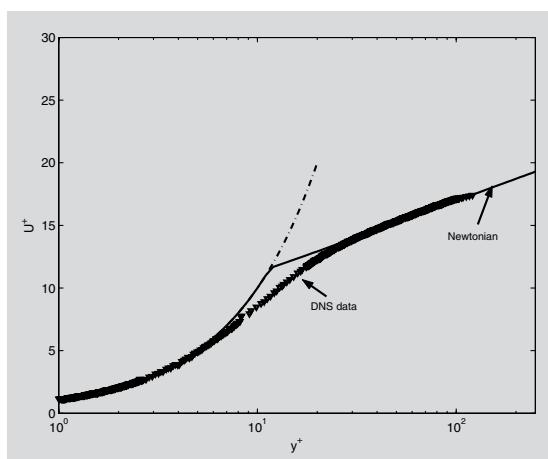
the inverse longest relaxation time, at least occasionally. The characteristic strain rate in an eddy is roughly the inverse of its turnover time. Thus, eddies whose turn-over time is longer than the fluid relaxation time, λ, will not have high enough velocity gradients to excite the polymer to cause it to stretch, and we expect that these eddies will be unaffected by the polymer. Hence, in order for an eddy of size r to have an influence on the polymer stretch, the following must hold:

$$\frac{\lambda}{\theta(r)} \geq 1$$

(35)

But if the polymer concentration is vanishingly small, its influence will be negligible, even if the chains are fully extended. So, the time scale criterion is not sufficient, by itself, to determine the level of drag reduction.

4.2 LENGTH-SCALE CRITERION

We now note that the stretching of polymers by the turbulent eddies enhances the extensional viscosity of the fluid. If the extensional viscosity becomes large enough, the eddies should begin to shut down, since very high extensional viscosities resist extensional flow, and vortices cannot exist without regions of extensional flow. The highest value of the extensional viscosity that can be attained is the asymptotic kinematic extensional viscosity, $\bar{\nu}_\infty$, when the chains are all fully extended. If the flow can stretch the polymer molecule completely, then the polymer will presumably have its maximum effect on turbulent structures. Of course, complete extension is improbable and we account for the partial stretching by $\bar{\nu}_e$, an effective extensional viscosity. We can make a similar argument for the case of fibers which are rigid rods to begin with, and so their maximum extensional viscosity is much more easily obtained than is the case for polymers. For fibers, the maximum extensional viscosity is attained as soon as the fiber axis has been rotated into the flow direction, while for
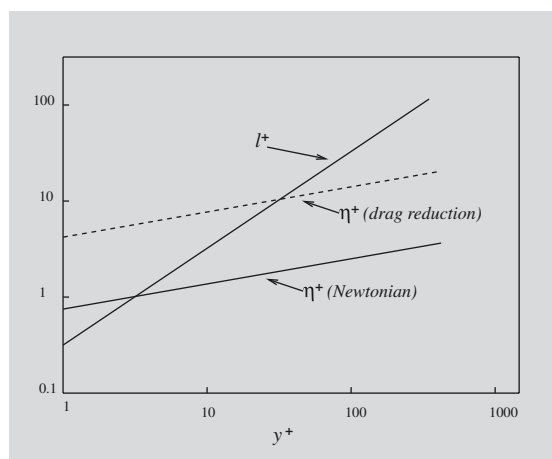
polymers, the chain must also be completely unraveled, a process that is strongly resisted by the entropic spring forces in the molecule. We note here that there are somewhat different values of the extensional viscosity depending on the type of extensional flow. However, for polymer or fiber, or any thread-like object, the maximum extensional viscosity varies by only an order unity prefactor among the various types of extensional flows, such as uniaxial, biaxial, or planar extension [46]. Thus, while recent work has implicated suppression of biaxial extensional flow as the primary means through which polymers on fibers suppress turbulent structures [47], our arguments are not sensitive to which kind of extensional flow is primarily suppressed.

In the buffer layer, the increased extensional viscosity should increase the dissipation length scale, or minimum eddy size at which turbulent energy is viscously dissipated, according to

$$\eta = \left(\frac{\overline{\nu}_e^3}{\langle \epsilon \rangle} \right)^{1/4}$$

(36)

where $\overline{\nu}_e$ is the increased extensional viscosity due to polymer stretch. This increase in the Kolmogorov length scale is illustrated in the upward shift of the dashed line in Fig. 6. If this minimum eddy size is not significantly smaller than the maximum eddy size, l, then we cannot be in the log region, because the large eddies can no longer simply hand off energy to smaller eddies, without feeling how these smaller eddies are influenced by viscous dissipation. That is, once the inertial cascade becomes shallow enough, there will be an influence of dissipation on the large eddies, presumably dampening their motion. This argument is akin to the hypothesis we made for the buffer layer in a Newtonian fluid, wherein we argued that in the buffer layer, the dynamics of the largest eddies must be affected by the smallest eddies due to the shal-

lowness of the cascade in this region. Recent direct numerical simulations have allowed more detailed insight by revealing that the most energetic coherent structures or the largest eddies in the near-wall regions are the quasi-streamwise rolls and that the polymer molecules are stretched by the extensional flow around these rolls [20]. It has also been shown both experimentally and by direct numerical simulations that polymer does indeed truncate the smallest scales of the turbulence, effectively increasing the size of the smallest eddies [35, 48].

If we assume that l remains unchanged even as the cascade is modified and consider it fixed, then from Eq. 30 it is clear that an increase in η will increase $\theta(l)$, the turnover time of the largest eddies. Hence, the stretching of polymers by the turbulent eddies will slow down the largest eddies. Qualitatively, we can see from Eq. 27 that such slowing down will decrease the eddy viscosity. Eq. 29 then tells us that the mean velocity gradient will therefore increase. It is clear from experiments that addition of polymer increases the average eddy size. This is modeled here by a selective suppression of the small eddies, leaving the larger eddies more prominent. It may be that, in addition, the largest eddies actually grow in size, but this is not considered in our model.

5 MEAN FLOW MODEL

We have now described qualitatively both the stretching of polymers by the eddies and its effect on the mean velocity profile. We therefore proceed to derive a mean flow model incorporating drag reduction. The streamwise mean momentum balance in drag-reduced channel flow has an additional polymer shear stress term:

$$-\rho \langle uv \rangle + \mu_o \frac{dU}{dy} + \Pi_{yx} = \tau_w \left(1 - \frac{y}{h} \right)$$

(37)

where Π_{yx} is the mean polymer shear stress. In order to calculate dU/dy from the above expression we model the Reynolds and polymer stresses together in terms of an eddy viscosity akin to the Newtonian case, a reasonable approximation to make in the regime of low to moderate drag reduction, wherein the polymer stresses account for less than 10% of the total stress balance over most of the channel cross-section (see Fig. 8b in [28]). Thus,

we have the following expression for the sum of the Reynolds and polymer stresses:

$$-\langle uv \rangle + \frac{\Pi_{yx}}{\rho} = v_{T,p} \frac{dU}{dy}$$

(38)

where $v_{T,p}$ is the eddy viscosity following drag reduction. Substituting Eq. 38 into Eq. 37 and assuming $y \ll h$ results in the following expression for the mean velocity profile, of the same form as the Newtonian case, only with $v_{T,p}$ replacing v_T:

$$\frac{dU}{dy} = \frac{u_T^2}{v_o + v_{T,p}}$$

(39)

Likewise, the expression for the largest eddy time scale in the Newtonian case, Eq. 30, carries over to the drag-reduced flow, except that the Kolmogorov length scale is now given by Eq. 36. We now utilize the time and length-scale criteria to develop an expression for $v_{T,p}$. We make note of the following assumptions:

1. The size of the largest eddies, l, remains unchanged even with polymer present.
2. Only eddies whose turnover time is smaller than the inverse of the longest relaxation time of the polymer will stretch the chains, i.e. the time-scale criterion must be met.
3. Once the polymer chains are stretched, they reduce turbulent drag due to an increase in the extensional viscosity leading to an enhancement in the size of the dissipative length scales.
4. Elasticity decreases the amount of drag reduction by allowing some of the energy transferred to the polymer by the turbulence to be transferred back to turbulent structures and re-energizing them.
5. In order to reduce turbulent drag, the dissipative scales must be increased in size sufficiently so that they can slow down the largest eddies; i.e. the Kolmogorov cascade must become shallow.
6. The enhanced extensional viscosity is the appropriate viscosity to use in order to compute the size of the polymer-modified dissipative (Kolmogorov) length scale.
7. The extent of polymer stretch is set by the ratio $\lambda/\theta(l)$, which is an effective Weis-

senberg number based on the largest eddy turnover time. This is a reasonable measure of the local flow strength - if the largest eddies are strong enough to stretch the polymer chains, then so will all smaller eddies since $\theta(l) < \theta(r) < \theta(\eta)$.

It is evident that the enhancement in the extensional viscosity of the fluid due to polymer stretch will be a fraction of the asymptotic extensional viscosity, which is the maximum possible enhancement. The increase in extensional viscosity at any y will be determined by the fluctuating extensional flow resulting from a coupling between the non-linear interactions and the mean shear in the buffer layer and log region [19, 20]. In our simple model, we account for this via the inverse of the largest eddy time scale, $1/\theta(l)$. So, we propose that the local extensional viscosity, $\bar{v}_e(l)$ to be given by the following phenomenological expression:

$$\bar{v}_e(l) = \bar{v}_\infty f\left(\frac{\lambda}{\theta(l)}\right) + 3v_s$$

(40)

where $f(\lambda/\theta(l))$ is an empirical function that varies smoothly between 0 and 1, representing the less than complete stretching of the polymer molecules by the flow due to elasticity. As a first guess, we will take for $f(\lambda/\theta(l))$ a hyperbolic tangent function, with a single parameter σ:

$$f\left(\frac{\lambda}{\theta(l)}\right) = \tanh\left(\frac{\lambda}{\sigma\theta(l)}\right)$$

(41)

Then, from Eqs. 23 and 36 the polymer-modified turbulent energy cascade becomes

$$\frac{\eta}{l} = \frac{\theta(l)^{1/4}}{lu_T^{1/2}}\left[\bar{v}_\infty \tanh\left(\frac{\lambda}{\sigma\theta(l)}\right) + 3v_s\right]^{3/4}$$

(42)

Since the expressions for the mean velocity profile for both the Newtonian, Eq. 29, and drag reduced flow, Eq. 39 are similar in form, substituting Eq. 42 into Eq. 30 gives us the following expression for the local polymer-modified largest eddy time-scale, scaled in turbulence wall time and length scales based on the zero-shear fluid viscosity - u^2_T/v_O and u_T/v_O, respectively:

$$\theta^{+}=\kappa y^{+}\left[1+\frac{\alpha}{\kappa y^{+}}\theta(l)^{1/4}\left\{Tr\,f\left(\frac{Wi_{\tau o}}{\sigma\theta^{+}}\right)+3\beta\right\}^{3/4}\right]$$

(43)

where κ = 0.4 is the von-Karman constant, α = 0.26 as calculated from numerical integration of the Newtonian mean velocity gradient in Eq. 32 and σ is a model parameter. The "Trouton ratio" Tr is here taken to be the maximum Trouton ratio, given by $Tr = \bar{v}_{\infty}/v_{O}$. Also in the turbulence wall time and length scales, v_{O} is the zero-shear kinematic viscosity of the solution. Note that in the above equation, the function f restricts the growth of θ^{+}. In this manner, we account for the fact that elasticity decreases the amount of drag reduction. The choice of function $f(Wi_{\tau O}/\sigma\theta^{+})$ should be such that it smoothly varies between $0 \leq Wi_{\tau O}/\sigma\theta^{+} < \infty$ with $f(0) = 0$ and $f(\infty) = 1$, so that for the case of a Newtonian fluid, Eq. 43 reduces to Eq. 31. We choose $f = \tanh$ and can now simultaneously solve Eq. 43 and integrate Eq. 32 to get the mean velocity profile in a drag-reduced wall-bounded flow. It should be possible to use this simple expression to solve for turbulent flow past a flat plate, including polymer injection and inhomogeneous polymer concentration fields.

To summarize, in order for visible polymer drag reduction to be observed, two criteria must be met. The first criterion, Eq. 35, is a time-scale criterion that tells us that unless the turnover time of the large eddies is fast enough compared to the polymer relaxation time to stretch the polymer, there will be no influence of the polymer. The second criterion, Eq. 42 and 43, says that even if polymer is stretched, it must increase the dissipation length scale enough to bring it near the length scale of the large eddies, so that their motion is slowed down. Obviously, neither is a completely "hard" criterion, but we expect that the influence of polymer on the flow will be controlled by the degree to which both of these criteria are met. If they are both well met out to some distance away from the wall, we expect that the production of turbulence in that region will be greatly reduced, the largest eddies will be slowed down and the mean velocity gradient will be substantially increased. Equations 43 and 32 reflect these changes. The two rheological variables that resulted from interpreting Virk's correlations, Tr and $Wi_{\tau O}$, naturally emerge in our model in the form

of length and time-scale criteria. However, our model does not predict a universal maximum drag reduction asymptote, wherein the mean velocity profile becomes independent of polymer characteristics and concentration. This was expected since we have not incorporated the physics of maximum drag reduction (MDR) into our model. Recently, attempts at explaining the particular shape and form of the MDR line as shown in Figs. 1 and 2 have been made by L'vov and co-workers [49] by considering an effective viscosity that varies linearly with the distance from the wall, $v_{eff} \sim y$ (As we explain below, our model and DNS data show decreasing polymer stretch with increasing distance y from the wall, in disagreement with the postulate of L'vov and co-workers.) Additionally, data shown in Berman [15] lies clearly above the universal MDR line.

It is instructive to explore the limit of Eq. 43 when $Tr \longrightarrow \infty$. This is the limit of the Oldroyd-B model, which represents the polymer as an infinitely extensible chain. In this limit, $\theta^{+} \longrightarrow \infty$, and Eq. 32 reduces to $dU^{+}/dy^{+} = 1$, which can be integrated to give $U^{+} = y^{+}$; the same mean velocity profile as the viscous sublayer. In other words, our phenomenological model predicts that for the case of drag reduction with Oldroyd-B model, at high Weissenberg number, the mean velocity profile over the entire channel is the same as the viscous sublayer. This result makes clear that our model applies only to the case of low and moderate drag reduction, and does not include the mechanism by which the drag reduction is limited at very high values of Tr and Wi.

We can, however, readily extend our model to fiber drag reduction. Since non-Brownian fibers are rigid, and do not need to be stretched, we do not need the function f to account for the partial stretch and elasticity as in the case of polymers and we replace the function f with a constant. Doing so allows us to derive the mean velocity profile in fiber drag reduction, in the same way as we did for polymers. The expression for θ^{+} becomes:

$$\theta^{+}=\kappa y^{+}\left[1+\frac{\alpha}{\kappa y^{+}}\theta(l)^{1/4}\left\{Tr\Upsilon+3\beta\right\}^{3/4}\right]$$

(44)

where Υ is another model parameter specific to fiber drag reduction. The above expression, when solved in conjunction with Eq. 32, gives us the
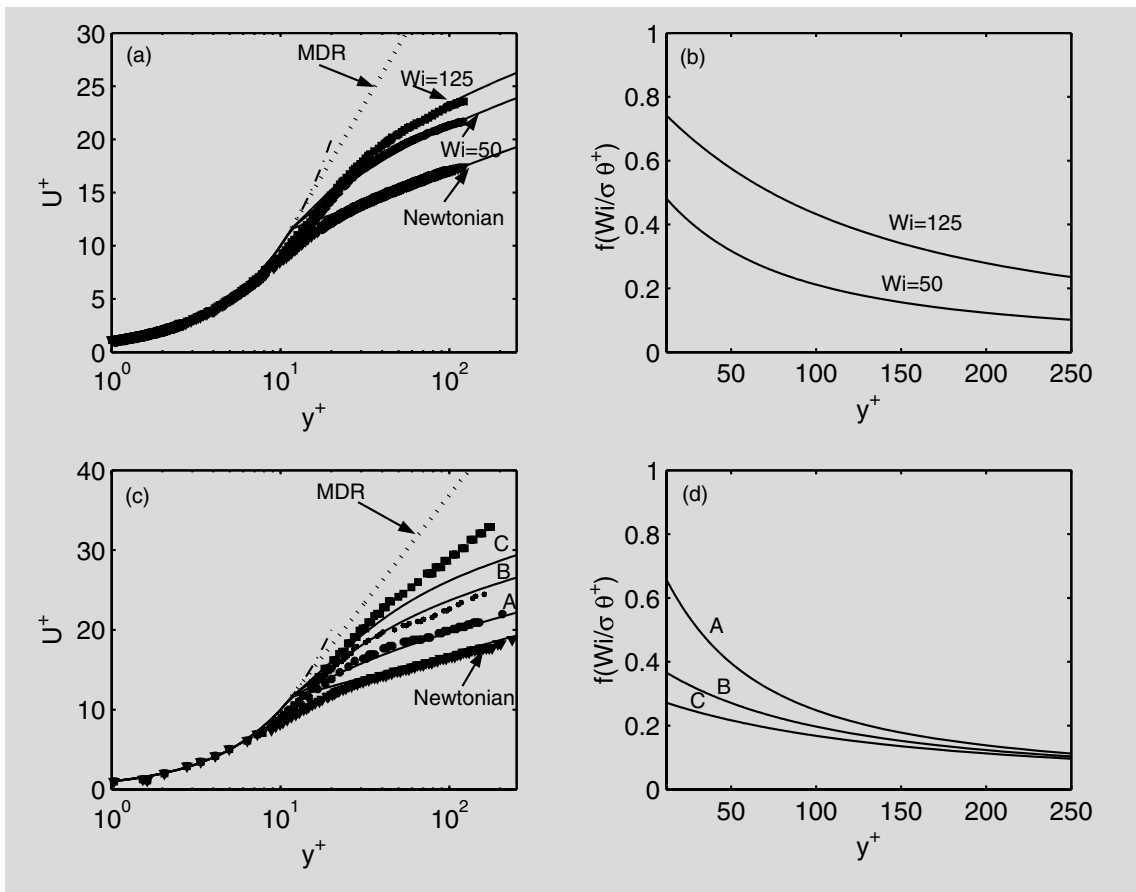
mean velocity profile with fiber drag reduction. No time-scale criterion is required for the case of non-Brownian fibers since the Peclet number, which is the ratio of the strain rate that orients a fiber to its rotary diffusivity which disorients it, is very large. Hence, fibers are quickly aligned in the flow and the alignment remains unaffected by Brownian motion. The length-scale criterion still needs to be met, however, which explains the appearance of *Tr* in Eq. 44.

6 DISCUSSION

6.1 COMPARISON WITH DNS AND EXPERIMENTAL DATA FOR POLYMER DRAG REDUCTION

The mean velocity profiles computed from our model are compared with DNS data in figure 7 (a & c). Except for a small region at the bottom of the buffer layer, the model compares remarkably well with data for different *Tr* and $Wi_{\tau O}$. In the simulations the polymer is represented by a finitely extensible dumbbell model (FENE-P), for which the Trouton ratio is given by:

$$Tr = 2(1 - \beta)b \tag{45}$$

where, $\beta = \mu_s/\mu_O$ as defined earlier. Also, *b* is the chain extensibility defined as $b \equiv 3L^3/\langle R^3 \rangle_O$, *L* being the fully stretched length of the polymer

chain and $\langle R^3 \rangle_O$ the equilibrium mean square end-to-end distance. Using the calculated values of *Tr* from Eq. 45 and the values of β, *b* and $Wi_{\tau O}$ specified in the DNS studies, the mean velocity profiles are generated. For a typical curve shown in Fig. 7a, $Wi_{\tau O} = 125$, *b* = 900, and $\beta = 0.9$ giving *Tr* = 180 from Eq. 45. Then using the same value of $\sigma = 0.22$, the curves shown in Fig. 7c can be generated by solving Eqs. 32 and 43.

A similar procedure has been used to generate the curves of Figs. 7c and 7d, where we see that our model is unable to predict the simulation results near MDR flow conditions on the PK plot, a cartoon of which is shown in Fig. 3. Curve "C" in Fig. 7c suggests that the mean velocity profile undergoes a permanent change in slope even before MDR, which is not captured by our model, at this point. In Fig. 7b and 7d we have plotted the degree of polymer stretch as a function of the distance from the wall, predicted by our model, which uses the function $f(\lambda/\theta(l)) = \tanh(Wi_{\tau O}/\sigma\theta^+)$ to determine the degree of polymer stretch by the mean flow. Notice that the stretch is highest near the wall and decreases monotonically away from the wall, in semi-quantitative agreement with DNS [21, 28].

Comparing the predictions of our model with experimental results is more difficult. Given all the uncertainties associated with the experimental data, namely unknown polydispersity of
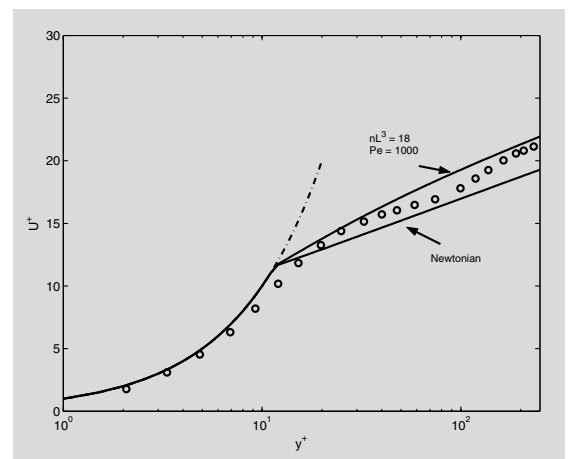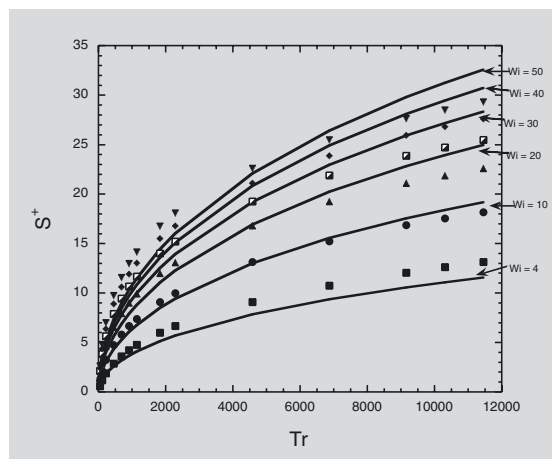
polymer, poor characterization of polymer solution and mechanical degradation of polymers in turbulence, it would be a miracle if any (and not just our) mean velocity profile model matched all the experimental data available. So here, we adopt an indirect method, in which we compare our model predictions against Virk's correlations that summarize many sets of drag reduction data, from which we can compute Tr from Eq. 21. Also from the intrinsic viscosity of the polymer solution, we can compute the longest relaxation time from Eq. 12, specifying the value of K_λ that is appropriate for the polymer-solvent pair. For instance, if we consider polyethylene oxide (PEO) with M_w = 5·10^6 g/mol in water at 298 K, for which the intrinsic viscosity $[\mu]_O$ = 1120 cm^3/gms, and assuming K_λ = 2, since water has a solvent quality that lies between good (for which K_λ = 2.369) and theta (for which K_λ = 1.69) [50] quality for PEO, then the relaxation time is computed to be λ = 10^{-3} s . If we assume polymer concentration to be c = 2.5 ppm, then Tr = 900 from Eq. 21. For typical values of u_T in lab-scale experiments we can then compute $Wi_{\tau O} \equiv \lambda u_T/\nu_O$. Assuming that $Wi_{\tau O} = Wi^*_{\tau O}$ = 1 at the onset of drag reduction, we can now use Eq. 10 to calculate the value of S^+.

We then feed in the same values of Tr, $Wi_{\tau O}$ and β into our model to compute the mean velocity profile corresponding to a given experimental condition. Since our model also asymptotes to a parallel-upward shifted mean velocity profile far away from the wall, we derive S^+ for our model and compare it to that predicted by Virk's expression in Fig. 8. Given its simplicity and the use of only one parameter, σ, our model does reasonably well in predicting S^+. We want to highlight that we have used the same value of σ = 0.5 for each data set in Fig. 8, but this value of σ is different (by a factor of two) from the one we used for comparison with DNS. In our opinion, this has to do with the artificially large $Wi_{\tau O}$ and the low values of Tr used in DNS, relative to the typical values in the experiments. Also, in DNS, an over-

simplified constitutive equation (FENE-P model) is used, and the molecules are taken to be monodisperse. These factors no doubt limit the degree to which the DNS results are able to model quantitatively the experiments, and the ability of own phenomenological model to describe both experimental and DNS results with the same value of σ.

6.2 COMPARISON WITH DNS FOR FIBER DRAG REDUCTION

For fiber drag reduction, we only have a single DNS result with which to compare [17]. No widely-cited experimental phenomenological relationships, similar to Virk's correlations, exist for fiber drag reduction and hence even indirect comparison with experiments is difficult. So, here we optimize our model for fiber drag reduction by setting a single value of Υ to match as well as possible the model predictions with the extent of drag reduction listed in Table 5 of [17]. This yields Υ = 18. Using the values of nL^3 in that table, we use Eqs. 19 and 21 to compute Tr, feed the result into Eq. 44, and solve for the mean velocity profile using the value of Υ = 18. We then integrate the resulting mean velocity profile and calculate the channel size required to obtain the specified Re_{mean} in Table 5 of [17]. The results are listed in Table 1. We can also use the same value of Υ = 18 and compare the mean velocity profile obtained from DNS for fiber drag reduction as shown in Fig. 9.

Note that the function f used in the case of polymer drag reduction ranges between 0 and 1, yet the constant we replace it with for fiber drag reduction has the best fit value Υ = 18. However, we also notice that the Tr values for fibers are miniscule compared to that for polymers, e.g. the Trouton ratio of fibers used in fiber drag reduction experiments, $Tr_{fiber} \sim O(1)$ [13], whereas, the Trouton ratio of drag reducing polymers is $Tr_{polymer} \sim O(10^4 - 10^5)$ [1]. Thus, even when the polymers are fully extended so that f = 1, polymers are much less efficient drag reducers than are fibers,

nL^3	Tr	Re_{eff}	Drag reduction DNS (%)	Drag reduction phenomenological model (%)
5	0.5	7425	7.4	7.1
9	0.9	7301	13.2	11.6
18	1.8	7100	18.5	19.4
36	3.6	6707	26.2	30.2

Table 1:
A comparison of model with DNS for fiber drag reduction, $\Upsilon = 18$.

for a given value of Tr. The lower drag-reducing efficiency of fully stretched polymers relative to aligned fibers, at the same value of Tr, suggests again that the prime mechanism for drag reduction is viscous damping of turbulent eddies, and that the elasticity present in flexible polymers (and largely absent from fibers) impedes drag reduction rather than causing it.

7   CONCLUSION AND FUTURE WORK

We have shown how a rheological interpretation of the Virk phenomenology is consistent with a viscous mechanism for drag reduction with polymers. In our development of this mechanism, Virk's critical wall shear stress and its dependence on polymer molecular weight are interpreted as a critical Weissenberg number allowing satisfaction of a time-scale criterion for drag reduction. Virk's slope increment and its dependence on polymer concentration are interpreted as a Trouton extensional viscosity that sets a length-scale criterion for drag reduction.

Specifically, we hypothesize that if the turnover time of the large eddies is shorter than the polymer relaxation time (thus satisfying the time-scale criterion) then polymers will be stretched, increasing the extensional viscosity and rate of dissipation, thereby increasing the dissipative length scale and making the turbulence cascade shallower. Consequently, the largest eddies are slowed down, particularly the ones close to the wall where the the cascade is shallowest. Since the largest eddies determine the mean momentum balance, their slowing down results in a reduction in eddy viscosity. As a result, the rate of momentum transport in the wall-normal direction decreases, thereby changing the mean velocity profile. For the case of non-Brownian fibers, there is no time-scale criterion and only the length-scale criterion must be satisfied for drag reduction. This physical picture can be captured remarkably well by a simple model that we have constructed. For polymer drag reduction, the model requires Tr, β and Wi_{TO} as inputs obtainable from the physical properties of the polymeric fluid, and delivers the mean velocity gradient as an output. For fiber drag reduction, the model requires only Tr and β as inputs.

Given its simplicity and the use of just one fitting parameter, the model does remarkably well in predicting numerical and experimental mean velocity profiles for both polymers and fibers.

Our phenomenological theory is amenable to molecular interpretation, mechanistic testing using polymer and fiber DNS, and extensions to more complex flows, such as boundary-layer flows, and flows with curved geometries, or non-uniform polymer and fiber concentrations. We also note that Brownian fibers result in smaller drag reduction compared to non-Brownian fibers [17]. Our model should be able to capture this effect by the use of a Peclet number instead of a Weissenberg number in the argument of the function, f. Then, just as lower Weissenberg number in polymers leads to smaller drag reduction, so will lower Peclet number in fibers result in a similar effect. Future work will focus on testing these predictions by comparing in more detail our theory with both direct numerical simulations (DNS) of turbulent flows and experimental data for both pipe and boundary-layer flows, with and without polymer injection. We also hope that a more detailed understanding of the differences between polymer vs. fiber drag reduction, and the role of elasticity in the former, will lead to an explanation of the 18-fold higher impact of fibers on drag reduction than for polymers with the same asymptotic extensional viscosity. Also, we hope that our simple phenomenological model can be extended to provide a model for the high drag reduction regime and the maximum drag reduction asymptote.

ACKNOWLEDGEMENT

REFERENCES

[1] PS Virk. Drag Reduction Fundamentals. AIChEJ 21 (1975) 625–656.

[2] DM Bushnell, KJ Moore. Drag reduction in nature. Annu. Rev. Fluid Mech. 23 (1991) 65–79.

[3] EB Chen, AJ Morales, C Chen, AA Donatelli, WW Bannister, and BT Cummings. Fluorescein and Poly(Ethylene Oxide) hose stream additives for improved firefighting effectiveness. Fire Fighting 34 (1998) 291–306.

[4] BA Toms. Some observations on the flow of linear polymer solutions through a straight tube at large Reynolds number. Proc. First Intl. Congress on Rheology 11 (1949) 134–141.

[5] BA Toms. Early experiments on drag reduction by polymers. Phys. Fluids 20 (1977) S3–S5.

[6] GA Agoston, WH Harte, HC Hottel, WA Klemm, KJ Mysels, HH Pomeroy, and J. M. Thompson. Flow of gasoline thickened by napalm. Ind. Eng. Chem. 46(5):1017–1019, 1954.

[7] JL Zakin and HW Bewersdorff. Surfactant drag reduction. Rev. Chem. Eng. 14 (1998) 253–320.

[8] A Robertson, S Mason. The flow characteristics of dilute fibre suspensions. TAPPI J. 40 (1957) 326–334.

[9] I Radin, J Zakin, G Patterson. Drag reduction in solid-fluid systems. AIChE. 21 (1975) 358–371.

[10] W Lee, R Vaseleski, A Metzner. Turbulent drag reduction in polymer solutions containing suspended fibers. AIChE J. 20 (1974) 128–133.

[11] R Pirih, W Swanson. Drag reduction and turbulence modification in rigid particle suspensions. Can. J. Chem. Engng. 50 (1972) 221–227.

[12] PS Virk, DC Sherman, DL Wagger. Additive equivalence during turbulent drag reduction. AIChE J. 43 (1997) 3257–3259.

[13] S Sasaki. Drag reduction effect of rod-like polymer solutions. J. Phys. Soc. Japan 60 (1991) 868–878.

[14] JL Lumley. Drag reduction by additives. Ann. Rev. Fluid Mech. 1 (1969) 367–384.

[15] NS Berman. Drag reduction by polymers. Ann. Rev. Fluid Mech. 10 (1978) 47–64.

[16] WD McComb, KTJ Chan. Laser-Doppler anemometer measurements of turbulent structure in drag-reducing fibre suspensions. J. Fluid Mech. 152 (1985) 455–478.

[17] JS Paschkewitz, Y Dubief, CD Dimitropoulos, ESG Shaqfeh, P Moin. Numerical simulation of turbulent drag reduction using rigid fibers. J. Fluid Mech. 518 (2004) 281–317.

[18] M Tabor, PG deGennes. A cascade theory of drag reduction. Europhys. Lett. 2 (1986) 519–522.

[19] PA Stone, F Waleffe, MD Graham. Toward a structural understanding of turbulent drag reduction: Nonlinear coherent states in viscoelastic shear flows. Phys. Rev. Lett. 89 (2002) 208301.

[20] Y Dubief, CM White, VE Terrapon, ESG Shaqfeh, P Moin, SK Lele. On the coherent drag-reducing and turbulence-enhancing behavior of polymers in wall flows. J. Fluid Mech. 514 (2004) 271–280.

[21] KD Housiadas, AN Beris. Polymer-induced drag reduction: Effect of the variations in elasticity and inertia in turbulent viscoelastic channel flow. Phys. Fluids 15 (2003) 2369–2384.

[22] S Sibilla, A Baron. Polymer stress statistics in the near-wall turbulent flow of a drag-reducing solution. Phys. Fluids, 14 (2002) 1123–1136.

[23] KR Sreenivasan, CM White. The onset of drag reduction by dilute polymer additives, and the maximum drag reduction asymptote. J. Fluid Mech. 409 (2000) 149–164.

[24] T Min, J Yoo, H Choi, DD Joseph. Drag reduction by polymer additives in a turbulent channel flow. J. Fluid Mech. 486 (2003) 213–238.

[25] T Min, J Yoo, H Choi, JY Yoo. Maximum drag reduction in a turbulent channel flow by polymers. J. Fluid Mech. 492 (2003) 91–100.

[26] JMJ den Toonder, MA Hulsen, GDC Kuiken, FTM Nieuwstadt. Drag reduction by polymer additives in a turbulent pipe flow: numerical and laboratory experiments. J. Fluid Mech. 337 (1997) 193–231.

[27] R Sureshkumar, AN Beris, RA Handler. Direct numerical simulation of turbulent channel flow of a polymer solution. Phys. Fluids 9 (1997) 743–755.

[28] PK Ptasinsky, BJ Boersma, FTM Nieuwstadt, MA Hulsen, BHAA van den Brule, JCR Hunt. Turbulent channel flow near maximum drag reduction: simulations, experiments and mechanisms. J. Fluid Mech. 490 (2003) 251–291.

[29] JMJ den Toonder, FTM Nieuwstadt, GDC Kuiken. Th role of elongational viscosity in the mechanism of drag reduction by polymer additives. Appl. Sci. Res. 54 (1995) 95–123.

[30] PJ Schmid, DS Henningson. Stability and Transition in Shear Flows. Springer Verlag, New York (2001).

[31] R Govindarajan, VS L'vov, I Procaccia. Retardation of the onset of turbulence by minor viscosity contrasts. Phys. Rev. Lett. 87 (2001) 174501–1.

[32] PA Stone, A Roy, RG Larson, F Waleffe, MD Graham. Polymer drag reduction in exact coherent structures of plane shear flow. Phys. Fluids 16 (2004) 3470–3482.

[33] F Waleffe. On a self-sustaining process in shear flows. Phys. Fluids 9 (1997) 883–900.

[34] J Jimenez, A Pinelli. The autonomous cycle of near-wall turbulence. J. Fluid Mech. 389 (1999) 335–359.

[35] MD Warholic, H Massah, TJ Hanratty. Influence of drag-reducing polymers on turbulence: effects of Reynolds number, concentration and mixing. Experiments in Fluids, 27 (1999) 461–472.

[36] GL Donohue, WG Tiederman, MM Reischman. Flow visualization of the near-wall region in a drag-reducing channel flow. J. Fluid Mech. 56 (1972) 559–575.

[37] Krope A, Krobe J, Lipus LC. A Model for Velocity Profile in Turbulent Boundary Layer with Drag Reducing Surfactants. Appl. Rheol. 15 (2005) 152-159.

[38] JO Wilkes. Fluid Mechanics for Chemical Engineers. Prentice Hall, New York (1999).

[39] RB Bird, CF Curtiss, R Armstrong, O Hassager. Dynamics of Polymeric Liquids - vol.2, John Wiley (1987).

[40] GK Batchelor. The stress system in a suspension of force-free particles. J. Fluid Mech. 41 (1970) 545–570.

[41] G Ryskin. Turbulent drag reduction by polymers: A quantitative theory. Phys. Rev. Lett. 59 (1987) 2059–2062.

[42] V Tirtaatmadja, GH McKinley, JJ Cooper-White. Drop formation and breakup of low viscosity elastic fluids: Effects of molecular weight and concentration. Phys. Fluids, in press.

[43] H Tennekes, JL Lumley. A First Course in Turbulence. MIT Press (1972).

[44] SB Pope. Turbulent Flows. Cambridge University Press (2000).

[45] AS Monin, AM Yaglom. Statistical Fluid Mechanics: Mechanics of Turbulence. MIT Press (1965).

[46] RG Larson. Constitutive Equations for Polymer Melts and Solutions. Butterworth Publishers (1988).

[47] V E Terrapon, Y Dubief, P Moin, ESG Shaqfeh, SK Lele. Simulated polymer stretch in turbulent flow using Brownian dynamics. J. Fluid Mech. 504 (2004) 61–71.

[48] E De Angelis, CM Casciola, VS L'vov, R Piva, I Procaccia. Drag reduction by polymers in turbulent channel flows: Energy redistribution between invariant empirical modes. Phys. Rev. E 67 (2003) 056312–1.

[49] VS L'vov, A Pomyalov, I Procaccia, and V Tiberkevich. Drag reduction by polymers in wall bounded turbulence. Phy. Rev. Lett. 92 (2004) 244503.

[50] RG Larson. Structure and Rheology of Complex Fluids. Oxford University Press, New York (1999).